J Electroceram (2008) 21:178–183
DOI 10.1007/s10832-007-9108-4

Characteristics of ZnO thin film for film bulk acoustic-wave resonators

Kok-Wan Tay · Po-Hsun Sung · Yi-Cheng Lin · Tsung-Jui Hung

Published online: 7 April 2007

Abstract Highly *c*-axis-oriented zinc oxide (ZnO) thin films were deposited on Au electrodes by reactive radio frequency (RF) magnetron sputtering and their sputtering pressure on thin film bulk acoustic-wave resonator (FBAR) characteristics are presented. The evolution of the preferred orientation and the surface morphologies of the deposited ZnO films are investigated using X-ray diffraction, scanning electron microscopy, and atomic force microscopy measurement techniques. The result obtained in this study show that the ZnO films prepared using a lower sputtering pressure of 2×10^{-3} Torr have a strong *c*-axis orientation, promote smoother surface and higher resonance frequency. The experimental results demonstrate that the fabricated two-port FBAR using the optimum process parameters yields an effective electromechanical coupling constant (k^2_{eff}) of 2.8%, series quality factor (Q_s) of 436, and a parallel quality factor (Q_p) of 600.

Keywords Sputtering · Thin film · Surface roughness · Acoustic wave

K.-W. Tay (✉)
Department of Electrical Engineering,
Wu Feng Institute of Technology,
Chiayi 621,
Taiwan, Republic of China
e-mail: kwtay@ms26.hinet.net

P.-H. Sung
Industrial Technology Research Institute, ERSO/ITRI,
Rm. 502, Bldg. 52, Hsinchu 310, Taiwan, Republic of China

Y.-C. Lin · T.-J. Hung
Department of Mechatronics Engineering,
National Changhua University of Education,
Changhua 500, Taiwan, Republic of China

1 Introduction

The increasing demand of smaller and more capable mobile phones, wireless network notebook computers, global positioning system (GPS) receivers, and military applications of radio frequency has led to an explosive growth in wireless communications technology. This requirement for high-frequency resonators, filters, and duplexers capable of operating in the 0.5 to 10 GHz frequencies ranges. Conventionally, microwave ceramic resonators and surface acoustic wave (SAW) resonators have been applied in this frequency range. However, microwave ceramic resonators tend to be physically bulky, while SAW resonators demonstrate a relatively poor sensitivity to temperature and have high insertion losses and limited power handling characteristics. Moreover, SAW devices must generally be interfaced at the board level rather than directly at the chip level. Thin film bulk acoustic-wave resonators (FBARs) have been developed to address the limitations of these conventional devices. Compared to microwave ceramic resonators and SAW resonators, FBARs have the advantages of low cost and enhanced electrical performance and are characterized by low insertion losses, high power handling capabilities, and high frequency operation [1, 2]. Furthermore, the miniature scale of FBARs and the possibility of mounting them on Si or GaAs substrates permit their use within microwave monolithic integrated circuits (MMICs) [3].

Similarly to SAW devices, an FBAR exploits the piezoelectric effect to convert electrical energy into mechanical energy and vice versa. However, unlike SAW devices, when an RF signal is applied to the FBAR, this signal expands and contracts in the form of mechanical deformations of the entire piezoelectric bulk layer. The performance of the FBAR depends on the presence of a

Table 1 Parameters used for sputtering ZnO films.

Parameters	Values
Target	ZnO (99.999%)
Substract	Au/Cr/ Si_3N_4/Si
Substrate_to_target distance (mm)	70
Base pressure (Torr)	5×10^{-6}
Sputtering pressure (Torr)	2×10^{-3}, 8×10^{-3}, 12×10^{-3}
Sputtering power (W)	200
Substrate temperature (°C)	300
Ar:O_2 gas flow rate ratio (sccm)	4 : 6
Deposition rate (μm h^{-1})	0.87

large acoustic impedance mismatch on both sides of the piezoelectric material to trap energy, and hence, produce resonant characteristics. This requires either the use of a Bragg reflector on the lower side of the piezoelectric [4] or the inclusion of an air/crystal interface beneath the resonator.

ZnO (Zinc oxide) thin films have widely been used as SAW devices and bulk acoustic resonators due to its strong piezoelectric effect [5]. ZnO films can be deposited by variety deposition techniques, such as molecular beam deposition (MBE) [6], chemical vapor deposition (CVD) [7], and sputtering [8]. The most commonly used technique is sputtering because it is possible to obtain good orientation and uniform films close to single-crystal morphology even on amorphous substrate or at low substrate temperature. In this study, we investigates the influence of various sputtering pressure on the deposition of highly *c*-axis-oriented ZnO films on Au seed layers and studies the characterization of ZnO thin films for use in FBARs.

2 Experimental procedure

In this study, the various ZnO thin films were deposited using reactive RF magnetron sputtering system. The sputtering chamber housed a 7.62-cm-diameter 99.999% pure ZnO target disc with a thickness of 6 mm. The substrate was comprised of p-type silicon (100) with a low-stress silicon nitride (Si_3N_4) membrane and an Au/Cr seed layer. The chamber was initially evacuated to a base pressure of 5×10^{-6} Torr using a rotary mechanical pump and a turbo molecular pump. In each of the current experiments, the target was pre-sputtered for 10 min under an RF power of 200 W. High purity argon (99.999%) and oxygen (99.999%) gases with a flow rate ratios of 4:6 (sccm) were introduced into the sputtering chamber by a mass flow controller. The substrate temperature was monitored by means of a thermocouple and had been attained at 300°C. The detailed deposition parameters are summarized in Table 1.

Figure 1 presents a schematic overview of the current FBAR fabrication process. The substrate was initially cleaned using a Radio Corporation in America (RCA) cleaning operation, and a low-pressure chemical vapor deposition (LPCVD) process was then employed to deposit films of low-stress Si_3N_4 on both sides of the substrate. The upper Si_3N_4 (2,000 Å) layer subsequently served as a support membrane for the FBAR, while the lower layer acted as an etching mask.

As it is necessary to prevent energy leakage during operation, the FBAR must be acoustically isolated from the substrate. Consequently, having patterned the low-stress Si_3N_4 layer on the underside of the silicon substrate, the substrate was etched selectively in a KOH (potassium hydroxide) wet etching process to create a cavity under the piezoelectric-active area. An etchant concentration of 40% KOH with 30% of water at 80°C was utilized to etch the silicon substrate to an appropriate thickness at an etching rate along the (100) plane of approximately 0.9 μm/min.

A thin Au (950 Å) /Cr (50 Å) film was then deposited over the membrane layer using an electron beam evaporation process and patterned using lift-off photolithography to form a nucleating layer for oriented piezoelectric ZnO thin film growth and to serve as the bottom electrode. The deposition parameters such as power, Ar-flow rate, and deposition pressure were 250 W, 170 sccm, and 3.4×10^{-3} Torr, respectively. The (111) orientation of the gold seed layer promotes *c*-axis orientation of the ZnO film. It is noted that a very thin layer of chromium (Cr) was inserted under the gold seed layer to improve the adhesion of the latter to the low-stress Si_3N_4 membrane layer. A reactive RF magnetron sputtering process was then employed to deposit a thin ZnO

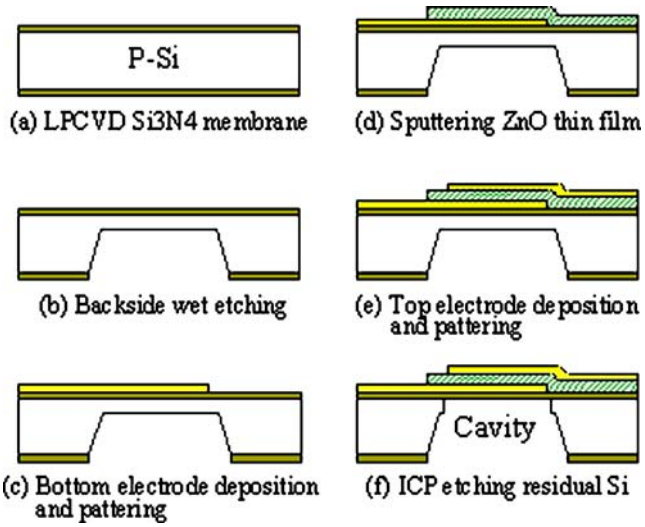

Fig. 1 FBAR fabrication process flow: (a) LPCVD low stress Si_3N_4 membrane, (b) Underside Si_3N_4 patterning and wet etching, (c) Au/Cr bottom electrode deposition and patterning, (d) ZnO film reactive sputtering and patterning, (e) Au/Cr top electrode deposition and patterning, (f) ICP etching residual silicon

film on the bottom Au/Cr electrode using the parameters described in Table 1. The ZnO thin film was then etched out in a solution of H_3PO_4:CH_3COOH:H_2O (1:1:40) without attacking the bottom electrode layer. An Au (950 Å)/Cr (50 Å) film was then evaporated on the ZnO film and patterned using lift-off photolithography to form the top electrode. Finally, an underside of the residual silicon wall was removed by an inductively coupled plasma (ICP) dry etching process to form a crystal/air interface beneath the resonator. As shown in Fig. 1(f), the FBAR fabricated using this process comprised a ZnO piezoelectric thin film sandwiched between two Au/Cr metal electrodes and supported on a low-stress Si_3N_4 membrane.

It is known that the preferred orientation and surface roughness of the deposited ZnO film have a significant impact on both the resonance properties and the reliability of the FBAR device. Therefore, this study analyzed the crystalline structures and crystallographic orientations of the ZnO films formed at different sputtering pressure conditions using an X-ray diffraction (XRD, RIGAKU D/max 2.B) technique performed with CuKá radiation (λ=1.5418 Å), a scanning range of 30 to 50°, and a scanning speed of 4°/min. Cross-section of the various ZnO film columnar structures were observed using scanning electron microscopy (SEM, PHILIPS XL-40FEG). A detailed analysis of the average peak to valley height of grain column and root-mean square (rms) surface roughness of each of the ZnO films was conducted using atomic force microscopy (AFM, SPA300HV) performed in the contact mode over a scanning area of 2 μm^2. The thickness of the films was determined using a stylus profilometer (Veeco DEKTAK). The *S* parameters were measured using a network analyzer (HP 8722ES) and a wafer probe station (Cascade Microtech).

3 Results and discussion

To study the feasibility of tuning, the sputtering pressure to obtain highly *c*-axis-oriented ZnO films, the present study developed ZnO films at a sputtering pressure of 12×10^{-3}, 8×10^{-3}, and 2×10^{-3} Torr, respectively. It is noted that in each case, the ZnO film thickness was approximately 1.3 μm, and the film was deposited over a period of 1.5 h.

To study the influence of the sputtering pressure on the crystallographic orientation of the ZnO films, Fig. 2(a) shows the diffraction pattern of the ZnO film deposited at a sputtering pressure of 12×10^{-3} Torr. It is noted that the remaining process parameters are as listed in Table 1. It can be seen that the intensity of the (002) peak located at 2θ= 34.42°, is relatively stronger than that of the Au (111) peak at 2θ=38°.

Figure 2(b) shows the diffraction pattern of the ZnO film deposited at sputtering pressure of 8×10^{-3} Torr. The experimental result indicates that compared to the previous case, the intensity of the (002) peak at 2θ=34.42° increases, while that of the Au (111) plane virtually disappears. When the sputtering pressure of deposition process is reduced to 2×10^{-3} Torr, Fig. 2(c) reveals that the intensity of the (002) peak is significantly enhanced. This indicates that the *c*-axis of the hexagonal ZnO structure is oriented perpendicularly to the substrate surface (the normal orientation), and hence, the piezoelectric qualities of the film are enhanced. The experimental results presented in Fig. 2 confirm that ZnO films prepared using a lower sputtering pressure (2×10^{-3} Torr) have a stronger diffraction intensity of the (002) peak than those prepared under the process with a higher sputtering pressure (12×10^{-3} Torr). Hence, utilizing a lower sputtering pressure improves the *c*-axis orientation of the ZnO film, which is beneficial, as the higher the *c*-axis orientation of a piezoelectric film, the higher the electromechanical coupling coefficient of the piezoelectricity [9].

Figure 3 presents SEM images of the cross-sectional structures of ZnO films deposited with the parameters described in Table 1. Figs. 3(a) to (b) show the case for deposition with a sputtering pressure of 12×10^{-3} and 8×10^{-3} Torr, respectively. The columnar structure is nevertheless formed, but the columnar structure is slightly slanted and causes the electromechanical coupling constant to become weak. Besides, the diameter of columns also increased and caused the surface morphology of the films to become coarser. Fig. 3(c) present the ZnO film grown using the lowest sputtering pressure of 2×10^{-3} Torr. The ZnO film has a typically oriented columnar structure in its initial growth stages and has a fine grain structure in the vicinity of the Au/Cr surface. The vertical columnar structures extend fully from the seed layer and clearly develop as the film thickness increases. This characteristic of the ZnO–Au/Cr

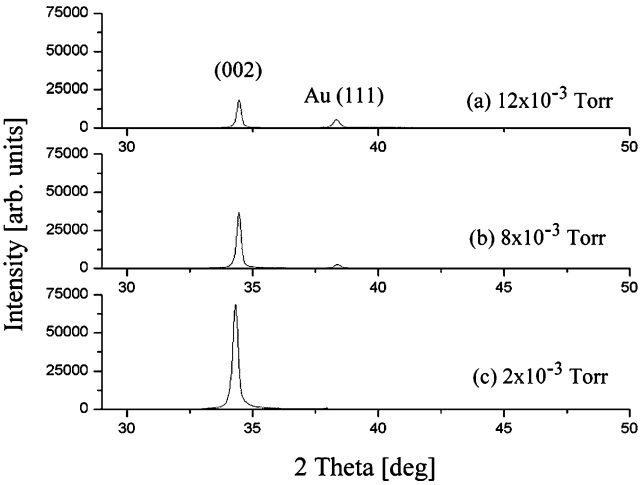

Fig. 2 XRD patterns of ZnO films deposited on Au/Cr seed layer at various sputtering pressures: (a) 12×10^{-3} Torr, (b) 8×10^{-3} Torr, and (c) 2×10^{-3} Torr

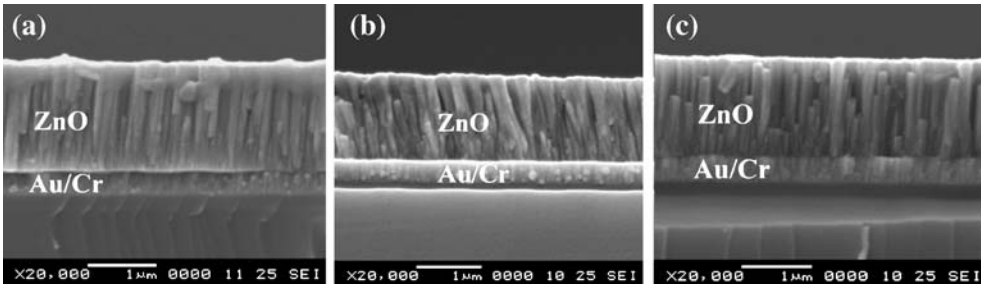

Fig. 3 The cross-sectional SEM images of ZnO films on Au/Cr seed layer at various sputtering pressures: (a) 12×10^{-3} Torr, (b) 8×10^{-3} Torr, and (c) 2×10^{-3} Torr

interface ensures good adhesion properties between the two layers and is indicative of a smooth interfacial quality in FBAR devices.

The fabricated ZnO films were measured using an AFM technique to gain a more meaningful insight into the surface roughness characteristics of each film. Figure 4 presents analysis of surface roughness and an average peak to valley height of ZnO films at various sputtering pressure. The results of Fig. 4 indicate that preparing ZnO films using a lower sputtering pressure of 2×10^{-3} Torr is found to have a root-mean square (RMS) value of 2.47 nm and an average peak to valley height of each grain column of 22.76 nm. It not only refines the film grain size, but also yields uniform films with smooth morphologies, and hence, improves the coupling factor when these films are utilized in FBAR devices. Figure 4 shows the case of the average surface roughness (RMS) and peak to valley height increase as the sputtering pressure increase. Consequently, it can be concluded that a higher sputtering pressure results in a large grain size and a rougher surface. This face was also confirmed by SEM measurement, as shown in Fig. 3.

Figure 5 shows the relationship between different sputtering pressures and resonance frequency. According to this figure, the thickness of low-stress Si_3N_4 membrane, ZnO film, and Au/Cr electrodes consisted of 0.2, 2.17, 0.1, and 0.1 μm, respectively. The experimental results indicate that the ZnO film prepared using the lower sputtering pressure of 2×10^{-3} Torr exhibits the higher resonance frequency. This demonstrates that the columnar structure, grain size, and surface roughness significantly affect the propagation loss and frequency response of a FBAR device.

The effective electromechanical coupling coefficient (k^2_{eff}) and the quality factor (Q_{f_x}) values are two fundamental indicators of the resonant performance of an FBAR. The effective electromechanical coupling coefficient is defined as [10]:

$$k^2_{\text{eff}} = \frac{\left(\frac{\pi}{2}\right)\left(\frac{f_s}{f_p}\right)}{\tan\left(\left(\frac{\pi}{2}\right)\left(\frac{f_s}{f_p}\right)\right)} \approx \left(\frac{\pi}{2}\right)^2 \frac{f_p - f_s}{f_p} \tag{1}$$

where f_p and f_s are the measured parallel and series resonance frequencies of the FBAR device, respectively. If a resonator is to be effective in a filter application, a wide gap should exist between its series and parallel resonant frequencies, i.e., the maximum bandwidth should be large.

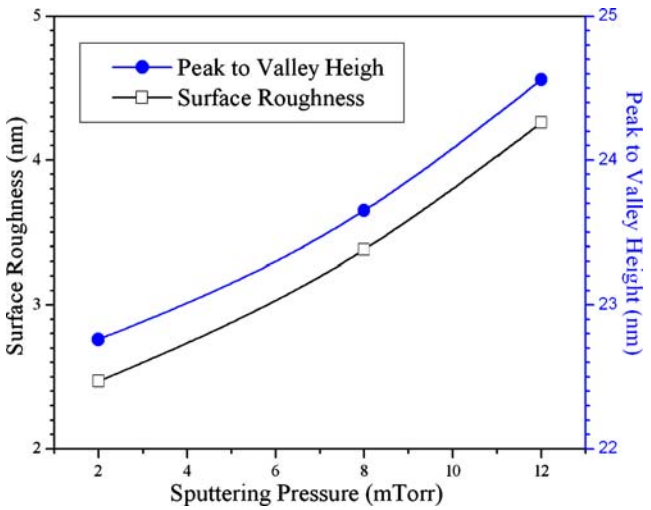

Fig. 4 Average surface roughness and peak to valley height of ZnO film deposited on Au/Cr layer at various sputtering pressure

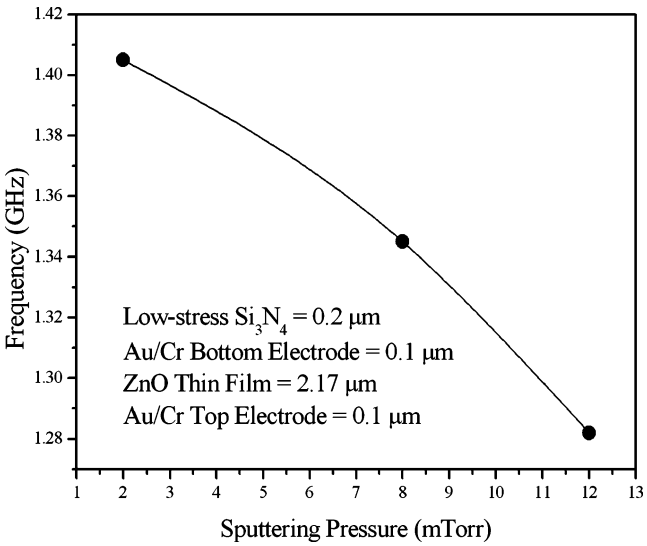

Fig. 5 Relationship between different sputtering pressure and resonance frequency

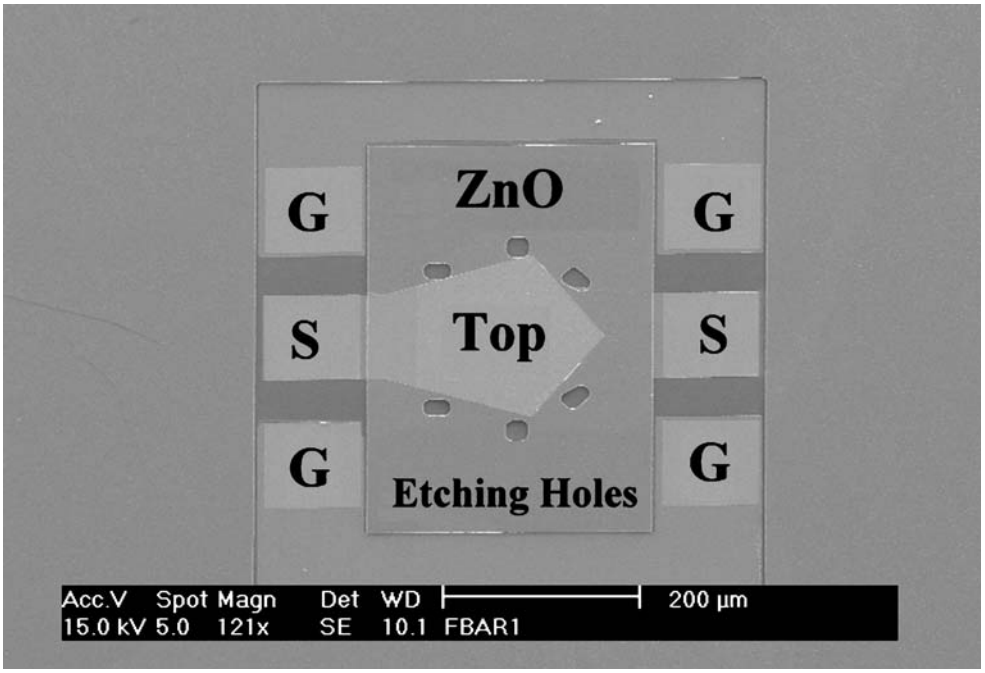

Fig. 6 SEM image of top view of fabricated two-port ZnO FBAR

The phase response can be differentiated. The quality factor (Q_{f_x}) is a measure of the acoustic loss in the device and can be expressed as [10]:

$$Q_{f_x} = \frac{f_x}{2}\left|\frac{d\angle Z_{in}}{df}\right|_{f_x} \quad (2)$$

where $\angle Z_{in}$ is the phase response in radians and f_x corresponds to either f_p or f_s.

To test the performance of the ZnO film in FBAR devices, a two-port FBAR device with four-layered composite structure was implemented and tested. The ZnO film was deposited using a lower sputtering pressure of 2×10^{-3} Torr process described above. Figure 6 shows the SEM image of the top view of the fabricated two-port ZnO FBAR. Its piezoelectric-active area (24,774 µm^2) was polygonal shape with five sides of 120 µm measured using G-S-G probe. The thickness of low-stress Si_3N_4 membrane, ZnO film, Au/Cr electrodes consisted of 0.2, 2.17, 0.1, and 0.1 µm, respectively. The phase and impedance measurements of the ZnO two-port FBAR are shown in Fig. 7. The phase rotation is not good due to the large electric resistance. The parallel and series resonance frequencies of the FBAR appeared at 1.415 and 1.395 GHz, respectively. For the current device, Equation 1 indicates that the effective electromechanical coupling coefficient is 2.8%, and the bandwidth is 20 MHz. Furthermore, Equation 2 reveals that the quality factors Q_s and Q_p is 436 and 600, respectively.

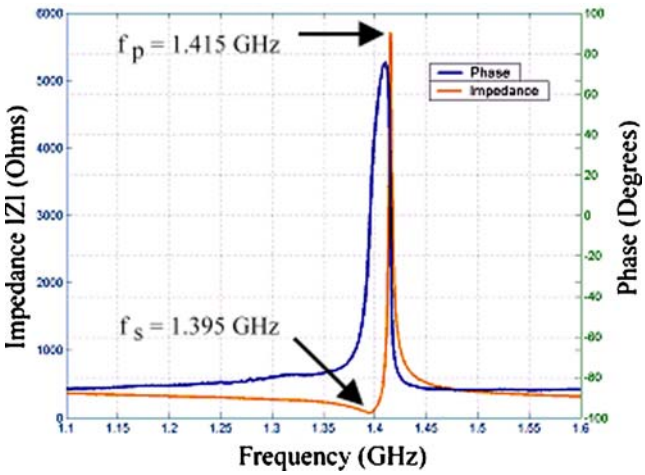

Fig. 7 Phase and impedance measurement of ZnO two-port FBAR

4 Conclusions

This study has used a reactive RF sputtering process to deposit highly *c*-axis-oriented ZnO thin films on Au/Cr seed layers for FBAR applications. It has been shown that the optimal growth conditions in a low-sputtering pressure of 2×10^{-3} Torr display a greater tendency to be aligned in the strongly preferred orientation toward the *c*-axis. Furthermore, these films possess smoother surface, a smaller grain size, and higher resonance frequency. The FBAR incorporating a ZnO film grown under optimal deposition parameters has an effective electromechanical coupling coefficient of 2.8% and a bandwidth of 20 MHz. Besides, the quality factors Q_s and Q_p are found to be 436 and 600, respectively. The present results provide a valuable contribution to the design of associated FBAR filters for wireless communication devices.

References

1. K.M. Lakin, G.R. Kline, K.T. McCrron, IEEE Trans. MTT-S Dig. **41**, 1517 (1993)
2. S.V. Krishnaswamy, J.F. Rosenbaum, S.S. Horwitz, R.A. Moore, IEEE MTT-S Dig. 153 (1992)
3. K.M. Lakin, J.S. Wang, G.R. Kline, A.R. Landin, Y.Y. Chen, J.D. Hunt. IEEE Ultrasonic Symp. Proceedings. (San Diego Ca, 1982), **1** p.466
4. K.M. Lakin, G.R. Kline, K.T. McCarron, IEEE MIT-S Digest. 833 (1995)
5. Q.X. Su, P. Kirby, E. Komuro, M. Imura, Q. Zhang, R. Whatmore, IEEE Trans. on Microwave Theory and Techniques. **49**, 769 (2001)
6. K. Nakamura, T. Shoji, K. Hee-Bog, Jpn. J. Appl. Phys., Part 2: Letters. **39**, L534 (2000)
7. T. Minami, H. Sonohara, S. Takata, H. Satu, Jpn. J. Appl. Phys., Part 2 Letters. **33**, L743 (1994)
8. Q.X. Su, P.B. Kirby, E. Komuro, R.W. Whatmore, IEEE/EIA Int. Freq. Contr. Symp. and Exhibition. 434 (2000)
9. M. Akiyama, H.R. Kokabi, K. Nonaka, K. Shobu, T. Watanabe, J. Am. Ceram. Soc. **78**, 3304 (1995)
10. J.L. Josept, S.N. Rajan, R. Rief, G.S. Charles. IEDM **96**, 4.4.1 (1996)